NUCLEOLAR REORGANIZATION AFTER CELLULAR STRESS IS ORCHESTRATED BY SMN SHUTTLING BETWEEN NUCLEAR COMPARTMENTS

Shaqraa Musawi[1,2], Lise-Marie-Donnio[1*], Charlène Magnani[1], Olivier Binda[1,3], Jocelyn Côté[3], Patrick Lomonte[1], Pierre-Olivier Mari[1] and Giuseppina GIGLIA-MARI[1*]

1. Institut NeuroMyoGène-Pathophysiology and genetics of neuron and muscle (INMG_PGNM), CNRS UMR 5261, INSERM U1310, Université de Lyon, Université Claude Bernard Lyon 1, Lyon, France
2. Department of Medical Laboratories Technology, College of Applied Medical Sciences, Jazan University, Jazan, Saudi Arabia.
3. University of Ottawa, Faculty of Medicine, Department of Cellular and Molecular Medicine, K1H 8M5, Ottawa, Ontario, CANADA

* Co-Corresponding authors

Keywords:

SMA, SMN, RNAP1, DNA repair, UV lesions, Nucleolus, Coilin, Fibrillarin

ABSTRACT

SMA is an autosomal recessive neuromuscular disease caused by mutations in the multifunctional protein SMN. Within the nucleus, SMN localizes to Cajal bodies (CBs), which have been shown to be associated with nucleoli, nuclear organelles dedicated to the first steps of ribosome biogenesis. The highly organized structure of the nucleolus can be dynamically altered by genotoxic agents. After a genotoxic stress, RNAP1, Fibrillarin (FBL) and nucleolar DNA are exported to the periphery of the nucleolus and once DNA repair is fully completed the organization of the nucleolus is restored. We found that SMN is required for the restoration of nucleolar structure after genotoxic stress. Unexpectedly, during DNA repair, SMN shuttles from the CBs to the nucleolus. This shuttling is important for the nucleolar homeostasis and relies on the presence of Coilin, FBL and the activity of PRMT1.

INTRODUCTION

The nucleolus is a nuclear membraneless organelle with a very structured internal organization, which associates with its different functions in ribosomal biogenesis: transcription of ribosomal DNA (rDNA) and early ribosomal RNA (rRNA) maturation [1]. Nucleoli are formed around the rDNAs which are composed by tandem head-to-tail repeats and their structure is thought to be strictly dependent on the transcriptional activity of the RNA polymerase I (RNAP1) [2]. Despite a very structured organization, nucleoli are very dynamic organelles, their shape and number can vary through the cell cycle and many proteins can enter or exit the nucleolus depending on physiological processes or cellular stress responses. This organized structure can be dynamically altered by both genotoxic agents and general cellular stress [3]. For instance, drugs that alter RNAP1 transcription (i.e. cordycepin, actinomycin D, etc.) may cause nucleolar segregation at the periphery of the nucleolus into structures known as nucleolar caps. Furthermore, drugs that block rRNA processing or the topoisomerase II (i.e. doxorubicin) but do not interfere with RNAP1 transcription induce a disruption of the compact nucleolar environment and nucleolar necklaces appear [4].

Amongst different cellular stresses known to modify nucleolar organization, UV-irradiation has the benefit of being a quick, punctual, and chemically clean method. Moreover, cells are able to repair UV-induced lesions and hence reverse their stress status. UV-induced DNA lesions are repaired by the Nucleotide Excision Repair system (NER)[5], which also repairs all bulky DNA lesions affecting the DNA structure, including environmental pollutants and the oxidative-damage derived cyclopurines [6].

During UV-irradiation, it has been showed that the nucleolus is not fully disrupted but nucleolar proteins (RNAP1, Fibrillarin [FBL]) and nucleolar DNA are exported to the periphery (for simplicity this phase will be called "displacement") of the nucleolus and when DNA repair is fully completed the proper nucleolar structure is restored (for simplicity this phase will be called "repositioning" [7]. Using a best candidate approach, we recently found that structural proteins like Nuclear Myosin I (NMI) and β-Actin (ActB) seem to play a prominent role in this process [8]. In cells depleted from NMI and ActB, nucleolar structure is not restored and both nucleolar proteins and nucleolar DNA remain at the periphery of the nucleolus, although DNA repair is completed and transcription is resumed [8]. However, the exact mechanism of NMI and ActB actions on nucleolar reorganization has not yet been elucidated, probably because many other molecular actors are still unknown. In order to find a complete molecular mechanism, several structural and nucleolar proteins have been scrutinized and a certain number have been found to be crucial to restore a proper nucleolar structure after DNA repair completion. One of these proteins is FBL. Consequently, we studied whether FBL interacting partners were also involved in this process. Amongst these different FBL partners, we investigated whether Survival of Motor Neuron (SMN) was implicated in the restoration of the nucleolar structure after DNA repair completion.

Spinal Muscular Atrophy (SMA) is an autosomal recessive neuromuscular disease, which affects neurons that controls the voluntary movement of muscles (motoneurons) [9]. In SMA, motoneurons are progressively lost leading to progressive muscle wasting and atrophy because muscles no longer receive signals from the motor neurons of the spinal cord. Children affected with SMA have symptoms that can vary greatly depending on the age of disease onset and its severity. Normal activities, such as crawling, walking, maintaining a seated position, controlling head movements, breathing and swallowing might be affected [9]. With an incidence of 1 in 6,000-10,000 live births, SMA is the most prevalent hereditary cause of infant mortality [10].

SMA is caused by bi-allelic mutations in the *SMN1* gene (Survival of Motor Neuron: SMN) and the disease phenotype is modified by the number of copies of a second paralog gene, *SMN2*, which is always present in SMA patients [11]. *SMN1* produces a full-length functional version of the SMN protein whereas in *SMN2*, the absence of exon 7 in most of the transcripts produces an unstable version of the SMN protein (SMNΔ7). *SMN2* can express about 10-15% of the full-length protein, which is insufficient to avoid the disease.

SMN is a multifunctional ubiquitous protein involved in many cellular processes, such as biogenesis and trafficking of ribonucleoproteins, local translation of messenger RNAs, etc [12]. SMN protein is ubiquitously expressed and is localized to both cytoplasm and the nucleus. Within the nucleus, SMN localizes in Gems and Cajal bodies (CBs), which have been shown to associate with nucleoli [13]. Within CBs, SMN interacts with the protein Coilin [14]. Interestingly, in certain conditions, SMN is also detected in nucleoli of mammalian primary neurons and colocalized with FBL [15]. In addition, a transient colocalization of SMN at the periphery of nucleoli with FBL after actinomycin D treatment in 10–20% of Hela cells [16,17] suggests that SMN could be present in the nucleolus under stress conditions. SMN Tudor domain is involved in the binding to RGG motifs containing proteins such as FBL and Coilin [18].

We investigated the possible role of SMN in nucleolar reorganization during both displacement and repositioning of RNAP1 during and after DNA repair of UV-induced damage and generally after stress induction. We show here that in the absence of a functional SMN, both RNAP1 and FBL remains at the periphery of the nucleolus after DNA repair completion even once transcription is fully restored. Interestingly, we could reveal a shuttling of SMN within the nucleolus after DNA repair and we determine that this shuttling is strictly dependent on physical interactions between SMN with FBL and Coilin. Moreover, arginine methylation reactions from PRMT1 governs this shuttling.

RESULTS

RNAP1 and FBL repositioning after DNA repair completion are SMN-dependent.

To investigate a possible role of SMN in nucleolar reorganization in response to cellular stress, we investigated whether the previously reported [7] RNAP1 UV-induced displacement and the later repositioning was still happening in absence of SMN. As SMN deficient cells we used both primary fibroblasts from SMA patients (Figure S1A) and transformed fibroblasts in which SMN was down regulated by lentiviral transfection of 2 independent inducible shRNAs against SMN 3'UTR (Figure S1B). Using these cell lines, we performed immunofluorescent (IF) assays to detect both RNAP1 and FBL positioning in the absence of damage (No UV), 3 hours post UV-irradiation (PUVI) (this time point corresponds to the minimum of RNAP1 transcriptional activity as found in [7] and at 40 hours PUVI (this time point corresponds to the RNAP1 full recovery of transcriptional activity and full DNA repair as described in [7]). Wild-type fibroblasts, SV40-transformed MRC5 and primary C5RO, were used as positive controls, while Cockayne Syndrome type B (CSB) TC-NER deficient fibroblasts (both transformed and primary; termed CSB-deficient) were used as negative control, as used in [7].

As described in [7], UV irradiation induced a displacement of both RNAP1 and FBL to the periphery of nucleoli in all cell lines tested (Figure 1A, 3h PUVI). As expected, in wild-type cells (MRC5, shSCRAMBLE and C5RO) both RNAP1 and FBL recovered their position within the nucleoli at 40 hours PUVI (Figure 1A). In contrast, in cells depleted of SMN (Figure 1A, Sh5-SMN and Sh6-SMN) or mutated in *SMN1* (Figure 1B, SMA1) neither RNAP1 nor FBL recovered the proper position within the nucleoli after DNA repair completion. As previously demonstrated [7], in CSB-deficient cells no return of the RNAP1 and FBL was observed (Figure 1A and B, CS1AN).

In CSB-deficient cells, the repositioning of RNAP1 and FBL is impeded because DNA lesions on the transcribed strand of rDNA genes are not properly repaired and RNAP1 transcription is not restored [7]. To investigate whether this was the case in SMN-deficient cells, we performed an RNA-fish assay detecting the pre-rRNA transcript using a specific probe against the 47S product (Figure S1C) and could determine (Figure S1D and S1E) and quantify (Figure 1C and D) that RNAP1 transcription is restored in SMN-deficient cells at 40 hours PUVI as in wild-type cells. In parallel, the involvement of SMN in Nucleotide Excision Repair (NER) is studied by performing UDS (Figure S2A), RRS (Figure S2B) and TCR-UDS (Figure S2C and S2D) experiments in cells depleted of SMN. Our results clearly show that SMN has no role in NER (Figure S2).

Taken together, these results indicated that in the absence of SMN, RNAP1 and FBL are correctly displaced at the periphery of the nucleolus in response to DNA damage but are not repositioned within the nucleolus once DNA repair reactions are completed and RNAP1 transcription is restored.

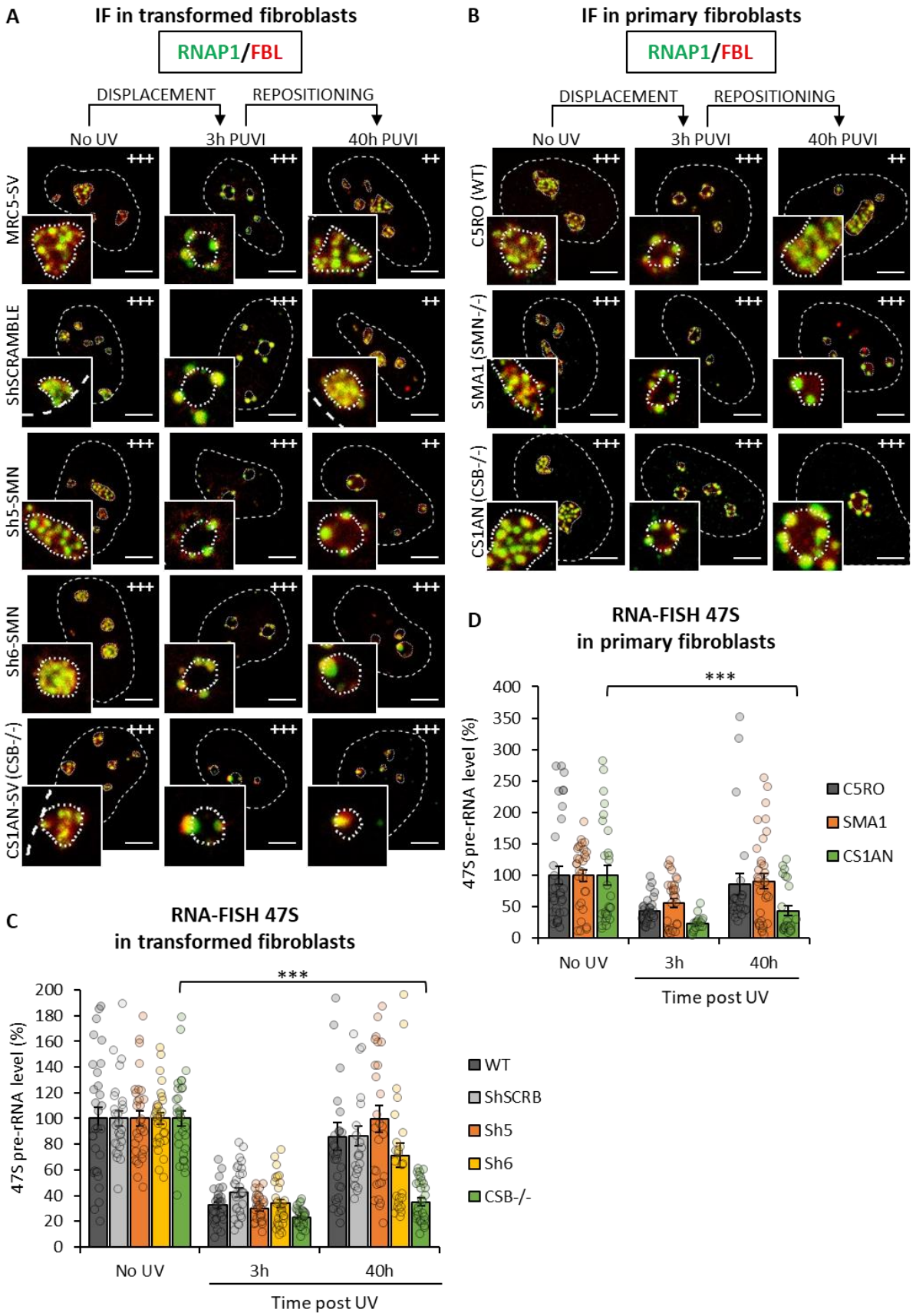
A
IF in transformed fibroblasts
RNAP1/FBL
DISPLACEMENT
REPOSITIONING
No UV
3h PUVI
40h PUVI
MRC5-SV
ShSCRAMBLE
Sh5-SMN
Sh6-SMN
CS1AN-SV (CSB-/-)
B
IF in primary fibroblasts
RNAP1/FBL
C5RO (WT)
SMA1 (SMN-/-)
CS1AN (CSB-/-)
C
RNA-FISH 47S
in transformed fibroblasts
47S pre-rRNA level (%)
***
No UV
3h
40h
Time post UV
WT
ShSCRB
Sh5
Sh6
CSB-/-
D
RNA-FISH 47S
in primary fibroblasts
47S pre-rRNA level (%)
***
No UV
3h
40h
Time post UV
C5RO
SMA1
CS1AN

129

Figure 1: RNAP1 and FBL movement during DNA repair in SMN deficient cells

(A and B) *Representative confocal microscopy images of immunofluorescence (IF) assay against RNAP1 (green) and FBL (red) in transformed* ***(A)*** *and primary* ***(B)*** *fibroblasts, different times post UV-irradiation (PUVI). Nuclei and nucleoli are indicated by dashed lines and dotted lines respectively. The number of the representative cells are indicated as followed + : 50–70%; ++ : 70–90%; +++ : >90%. Scale bar: 5 µm.* ***(C and D)*** *Quantification of RNA-FISH assay showing the 47S pre-rRNA level after UV-C exposure in transformed* ***(C)*** *and primary* ***(D)*** *fibroblasts. Error bars represent the SEM obtained from at least 27 cells. P-value of student's test compared to No UV condition: ***<0.001*

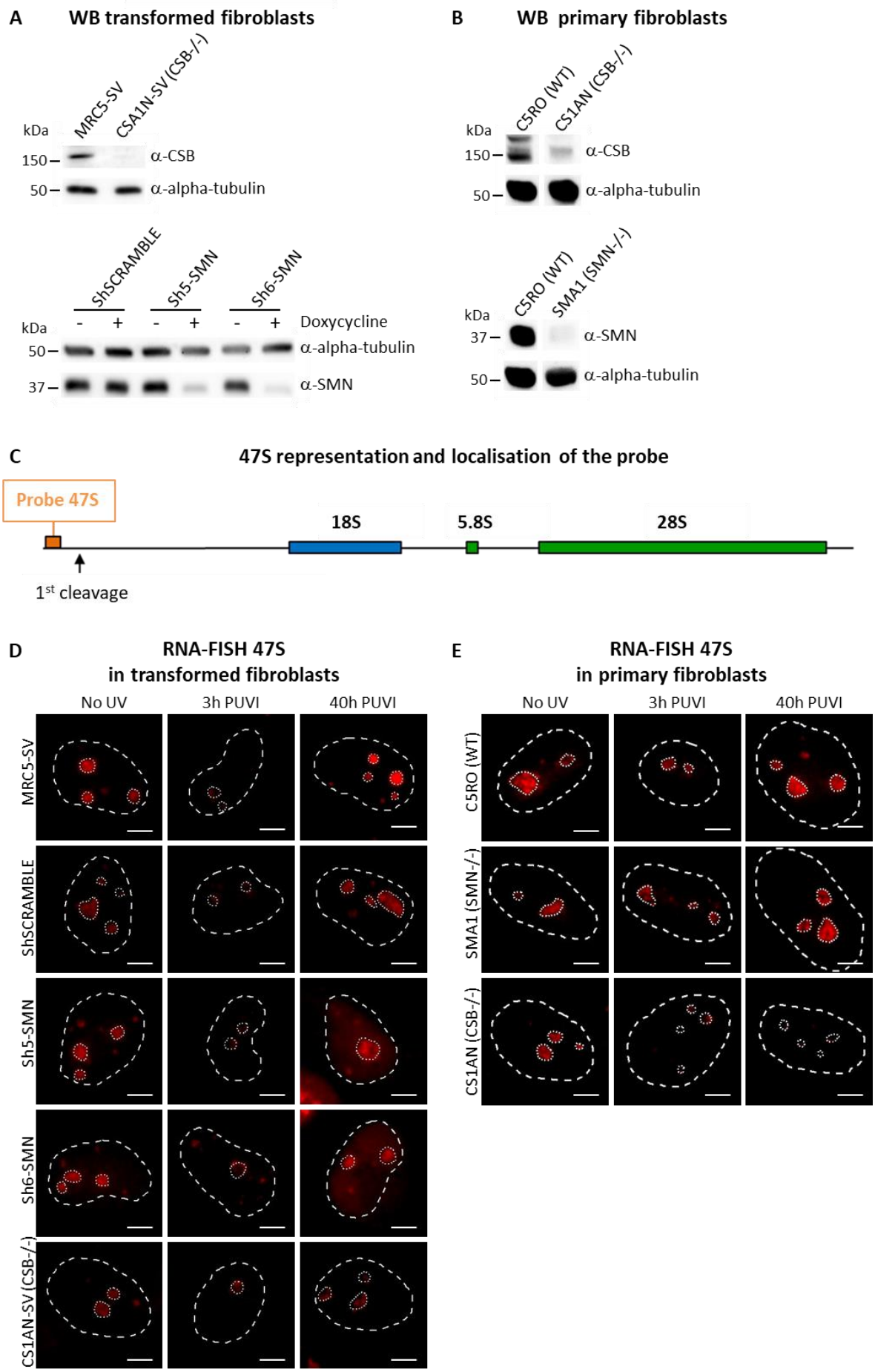
A
WB transformed fibroblasts
MRC5-SV
CSA1N-SV (CSB-/-)
kDa
150
50
α-CSB
α-alpha-tubulin
ShSCRAMBLE
Sh5-SMN
Sh6-SMN
- + - + - +
Doxycycline
α-alpha-tubulin
37
α-SMN
B
WB primary fibroblasts
C5RO (WT)
CS1AN (CSB-/-)
SMA1 (SMN-/-)
C
47S representation and localisation of the probe
Probe 47S
18S
5.8S
28S
1st cleavage
D
RNA-FISH 47S
in transformed fibroblasts
No UV
3h PUVI
40h PUVI
MRC5-SV
ShSCRAMBLE
Sh5-SMN
Sh6-SMN
CS1AN-SV (CSB-/-)
E
RNA-FISH 47S
in primary fibroblasts
C5RO (WT)
SMA1 (SMN-/-)
CS1AN (CSB-/-)

Figure S1: Western blot showing the reduction of SMN and representative images of RNA-FISH 47S in primary and transformed fibroblasts.

(A and B) *Western Blot of SMN and CSB on whole cell extracts of transformed cells* ***(A)****, and primary cells* ***(B).*** *Doxycycline treatment induce the expression of the ShRNA.* ***(C)*** *Schematic representation of rRNA unit and localization of the 47S pre-rRNA probe.* ***(D and E)*** *Representative images of RNA-FISH 47S in transformed fibroblasts from figure 1C* ***(D)*** *and in primary fibroblasts from figure 1D* ***(E)****. Scale bar 5µm*

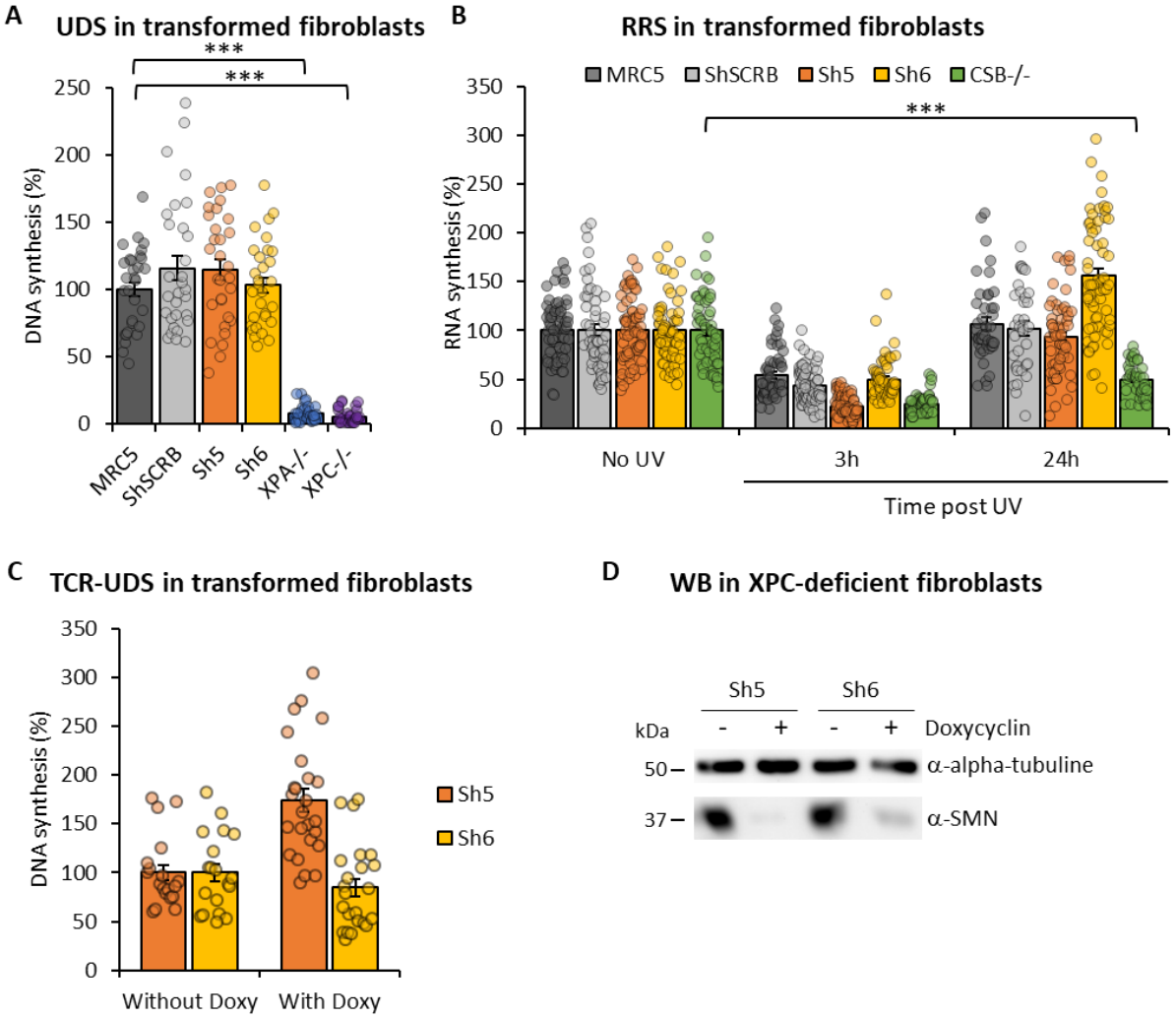

Figure S2: No role of SMN in NER

(A) *Quantification of Unscheduled DNA Synthesis assay (UDS) determined by EdU incorporation after local damage (LD) induction with UV-C (100J/m²) in transformed fibroblasts. Error bars represent the SEM obtained from at least 30 LDs.* ***(B)*** *Quantification of RNA Recovery Synthesis (RRS) assay determined by EU incorporation after UV-C (10J/m²) exposure in transformed fibroblasts. Error bars represent the SEM obtained from at least 50 cells.* ***(C)*** *Quantification of TCR-UDS assay determined by EdU*

incorporation after LD induction with UV-C (100J/m²) in GG-NER deficient cells (XPC-/- cells) expressing or not Sh5-SMN or Sh6-SMN. Error bars represent the SEM obtained from at least 15 LDs. ***(D)*** *Western Blot of SMN on whole cell extracts of XPC-deficient cells with sh5-SMN or sh6-SMN. The expression of the ShSMN is induced by doxycycline treatment.*

SMN-complex shuttles in the nucleolus and co-localizes with nucleolar proteins after UV irradiation.

We showed that SMN is required for the proper repositioning of RNAP1 and FBL at late time points PUVI. We questioned how SMN could be involved in this mechanism if usually it is not present in the nucleoli. In fact, SMN protein is typically located in the cytoplasm and within the nucleus where SMN is found in CBs together with Coilin and in Gems without Coilin. To study the localization of SMN and RNAP1 during the DNA repair process, we initially performed immunofluorescence assays at 3 hours and 40 hours PUVI in wild-type cells. Remarkably, at 40h PUVI, two co-existing populations of cells could be detected: (i) a majority of cells in which RNAP1 is repositioned within the nucleolus and SMN is localized in the CBs and (ii) a minority of cells in which RNAP1 is still localized at the periphery of the nucleolus and SMN is unusually localized within the nucleolus and cannot be detected in CBs anymore (Figure 2A, panel d and e). Because of this result, we decided to extend our analysis adding a time point intermediate between 3h and 40h PUVI (24 h PUVI) and a time point beyond the 40h PUVI (48h PUVI) and performed the IF assays against SMN and different nucleolar proteins or SMN protein partners (Figure 2). Importantly, we verified the RNAP1 transcriptional activity by RNA-FISH of 47S at 24h and 48h PUVI and show that RNAP1 transcription is not yet restored at 24h PUVI but it's fully recovered at 48h PUVI (Figure S3A). Surprisingly, at 24h PUVI, our results revealed the presence of SMN at the periphery of and/or within the nucleolus in the vast majority of cells (Figure 2A, panel c). Concomitantly, at 24h PUVI, RNAP1 was found to be localized at the periphery of the nucleolus (Figure 2A, panel c). On the other hand, we observed a complete return to the undamaged condition (RNAP1 within the nucleolus and SMN in the CBs) at 48h PUVI in the vast majority of cells (Figure 2A, panel f). Despite the presence of SMN and RNAP1 at the nucleolar periphery together at 24 h post-UV, any co-localization between these two proteins was observed (Figure 2A, panel c).

We showed that the loss of SMN alters FBL localization at 40 h PUVI (Figure 1A and 1B). Using GST pull-down assays we confirmed that FBL from cell extracts interacts with SMN [16,19,20] (Figure S3B). Furthermore, using a panel of SMA-linked TUDOR domain mutants, we established that FBL-SMN interactions require an intact TUDOR domain (Figure S3C). We therefore examined the localization of SMN and FBL during the DNA repair process (Figure 2B). Interestingly, we observed a substantial co-localization between SMN and FBL at 24 h PUVI within the nucleolus (Figure 2B panel i). The co-

localization can also be observed at 40 h PUVI in the population of cells that, at this time point, have not yet restored FBL position within the nucleolus (Figure 2B panel j).

In the absence of damage, SMN co-localizes and interacts with Coilin in CBs [14], however after DNA damage induction, it has been shown that CBs are disrupted [21]. Because of these evidences, we examined the localization of Coilin and its interactions with SMN during the DNA repair process. Interestingly, Coilin is localized to the periphery of the nucleolus already at 3h PUVI (Figure 2C, panel n) and remains in this location at 24h PUVI (Figure 2C, panel o) and at 40h PUVI (Figure 2C, panel p) in the subset of cells that did not yet repositioned RNAP1. Remarkably, when Coilin is at the periphery of the nucleolus it does not colocalize with SMN (Figure 2C, panel o and p).

Interestingly and differently from Coilin, at 3h PUVI, SMN is still visible in a focal pattern within the nucleus, reminiscent of Gems. Because of this Coilin-independent localization and to investigate whether SMN shuttles within the nucleolus as an individual protein or as a complex, we investigated whether Gemin5 (one of the subunits of the SMN complex) changes location after UV-irradiation. Remarkably, we could show that Gemin5 interacts with SMN all along this process of displacement and repositioning (Figure 2D), suggesting that it is not just SMN that shuttles in and out if the nucleolus, but that the whole SMN complex is likely involved in this process, or at least some components of the complex.

Moreover, to investigate whether the shuttling of SMN within the nucleolus is specific to UV damage or a general role in stress response, we treated the MRC5-SV cells with Cordycepin, a RNAP1 transcription blocking drug (FigureS4A) and examined the localization of SMN (Figure S4B). When treated with cordycepin, SMN shuttling into the nucleolus was also observed, although with faster kinetics than with UV (Figure S4B).

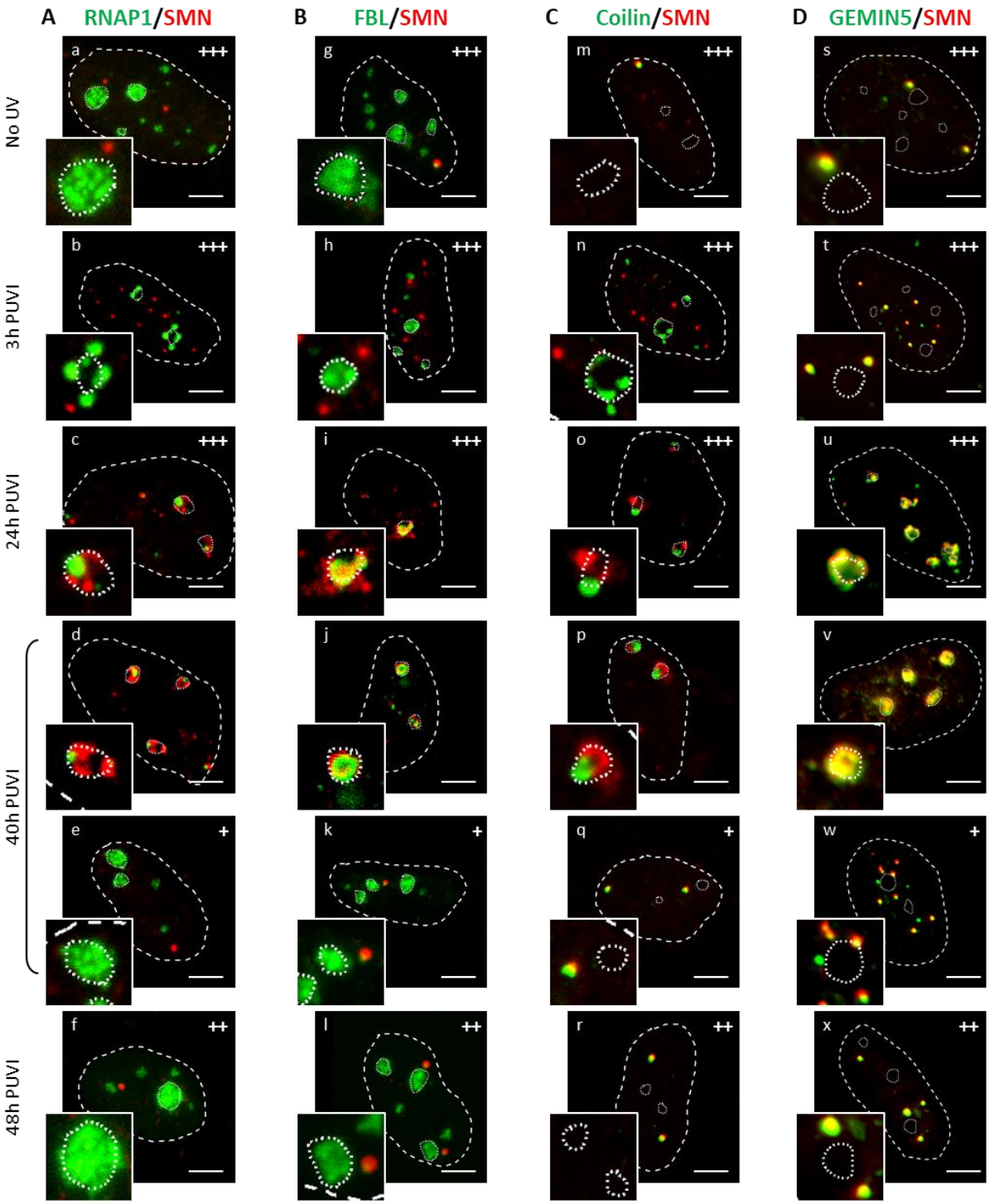

Figure 2: Movement of SMN and its partners during DNA repair

Representative confocal microscopy images of IF in MRC5 cells showing, after 16J/m² UV-C irradiation, the localization of SMN (red) and ***(A)*** *RNAP1,* ***(B)*** *FBL,* ***(C)*** *Coilin or* ***(D)*** *GEMIN5 (green). Nuclei and nucleoli are indicated by dashed lines and dotted lines respectively. The number of the representative cells are indicated as followed + : 50–70%; ++ : 70–90%; +++ : >90%. Scale bar represents 5 µm.*

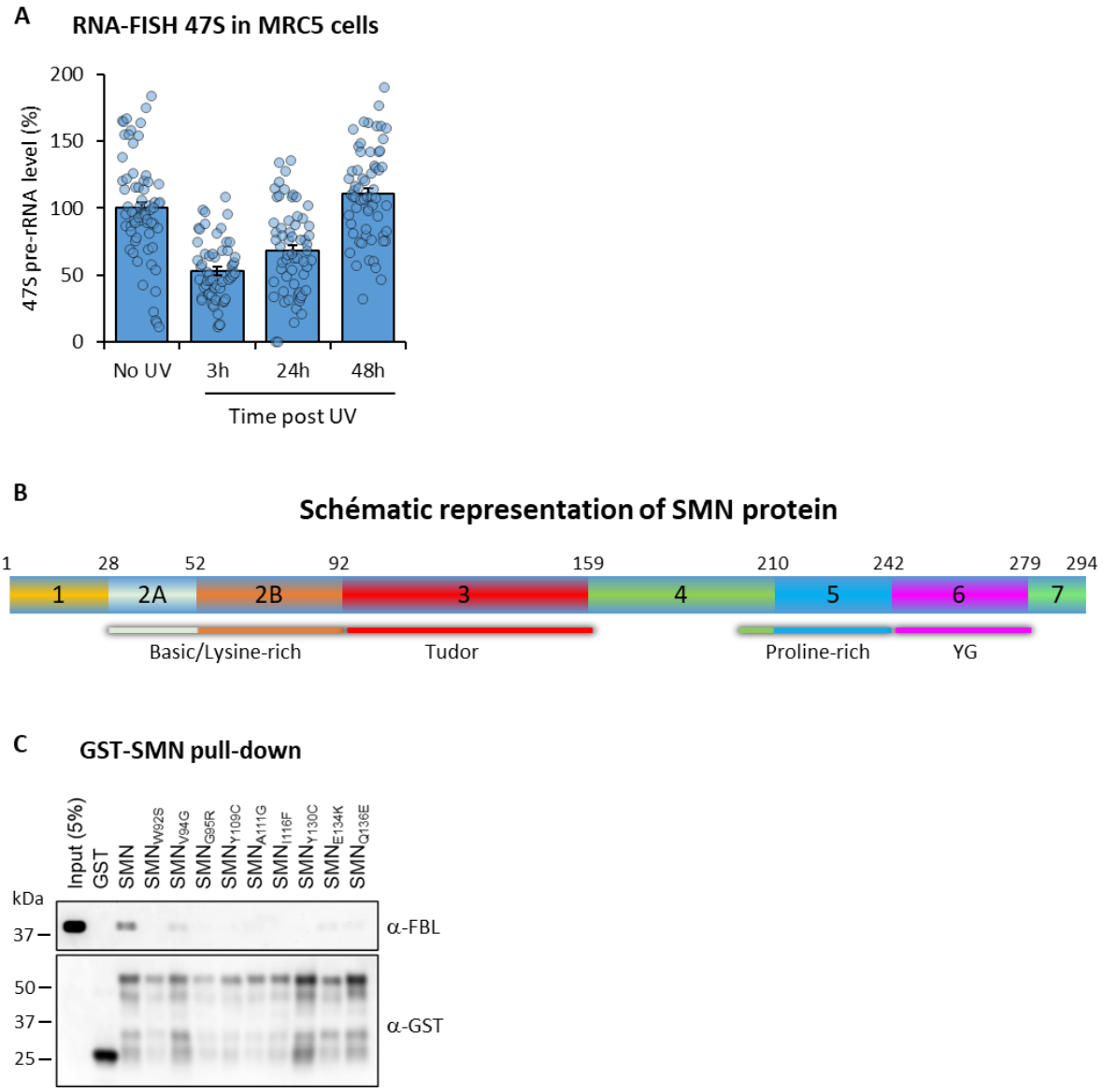

Figure S3: RNA-FISH 47S and GST pull-down of SMN and FBL

A) *Quantification of RNA-FISH assay showing the 47S pre-rRNA level in MRC5-SV cells after 3h, 24h and 48h of UV-C exposure (16J/m²). Error bars represent the SEM obtained from at least 50 cells.* ***B)*** *Schematic representation of SMN protein with the different exons as well as domains they encode which are shown as bars. Number of amino acids encoded by each exon is indicated.* ***C)*** *GST pull-down assay using purified recombinant SMN protein with different mutation in the Tudor domain found in SMA patients and cellular extracts.*

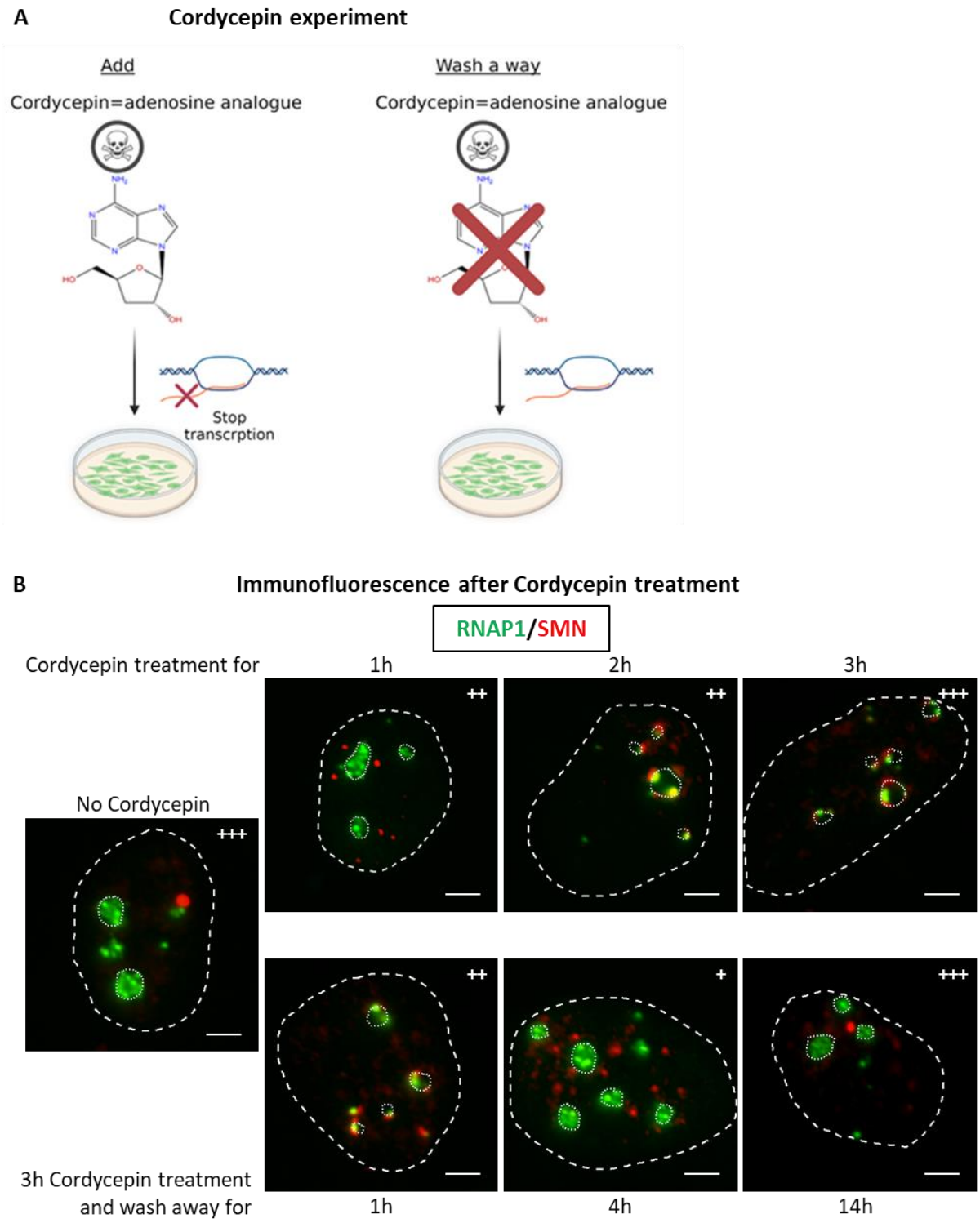

Figure S4: SMN Shuttle to the nucleolus after transcription blockage

(A) *Schematic representation of experiment using Cordycepin treatment.* ***(B)*** *Representative confocal images of IF against RNAP1 (green) and SMN (red). Nuclei and nucleoli are indicated by dashed lines and*

dotted lines respectively. The number of the representative cells are indicated as followed + : 50–70%; ++ : 70–90%; +++ : >90%. Scale bar represents 3µm.

SMN interacts with FBL inside nucleolus after UV irradiation in vivo and in vitro.

We showed that SMN co-localizes with FBL within the nucleolus at 24h PUVI. To assess the in vitro interaction between SMN and FBL after UV-C exposure, we performed GST pull-down assay using cell extracts untreated or UV-treated at different time points (Figure 3C). We observed that UV treatment seemed to enhance FBL-SMN interactions, while GST alone failed to associate with FBL even if more GST alone than GST-SMN was used in pull-down assays. To confirm this result in vivo, we performed a Proximity Ligation Assay (PLA) on wild-type cells at different time PUVI (Figure 3A). The majority of the cells at 24h PUVI presented a strong PLA signal specifically in the nucleolus between SMN and FBL, this signal persisted at 40h and 48h PUVI (Figure 3A and 3B).

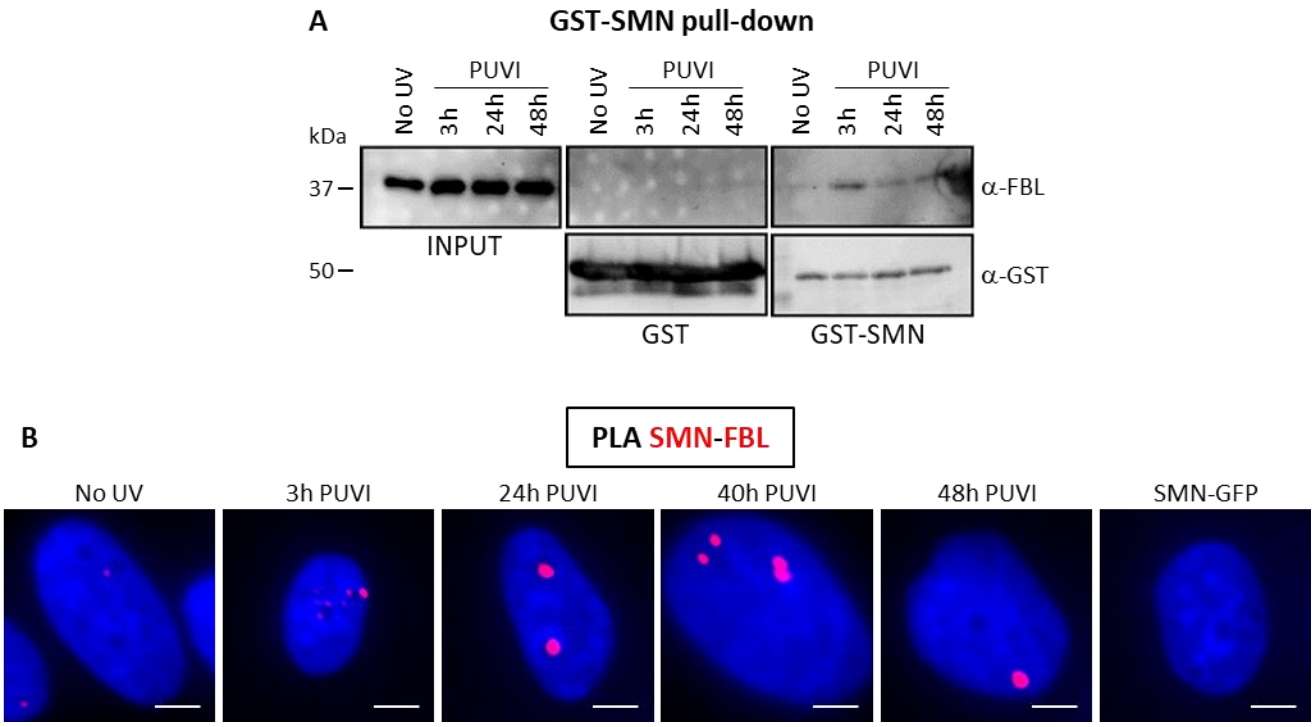

Figure 3: SMN interacts with FBL after UV irradiation.

(A) *GST pull-down assay using purified recombinant SMN protein and cellular extracts after UV-C irradiation.* ***(B)*** *Representative microscopy images of proximity ligation assay (PLA) showing the interaction between FBL and SMN in WT cells after UV-C irradiation. Scale bar: 5µm.*

Coilin is required for SMN import into the nucleolus and for the nucleolar rearrangement following UV-C exposure.

We observed that Coilin localized to the nucleolus during UV damage before SMN (at 3h PUVI) (Figure 2C). These results led us to hypothesize that Coilin is the factor that recruits SMN to the nucleolus. To test this idea, we depleted cells of Coilin by using a pool of four specific siRNAs (Figure 4D) and performed IF of SMN and RNAP1 on wild-type cells before damage and at different time PUVI (Figure 4A) in presence or absence of Coilin. Our results show that, without Coilin, the shuttling of SMN within the nucleolus is impaired and SMN remains in the nucleus at any time points (Figure 4A, siCoilin). Consequently, in cells deficient for Coilin, the nucleolar reorganization after DNA damage and repair is not repristinated and RNAP1 remains at the periphery of the nucleolus at 48h PUVI, indicating that the shuttling of SMN and the presence of Coilin are both important to insure the reestablishment of the nucleolar reorganization.

To investigate whether the absence of Coilin would impact the interaction between SMN and FBL, we performed PLA and IF of SMN and FBL on wild-type cells before damage and at different time PUVI in presence or absence of Coilin (Figure 4B and 4C). Our results show that without Coilin, SMN remaining outside of the nucleolus, no co-localization with FBL was observed (Figure 4B). By consequence, the interaction between SMN and FBL observed at 24h and 40h PUVI is lost in Coilin-depleted cells (Figure 4C).

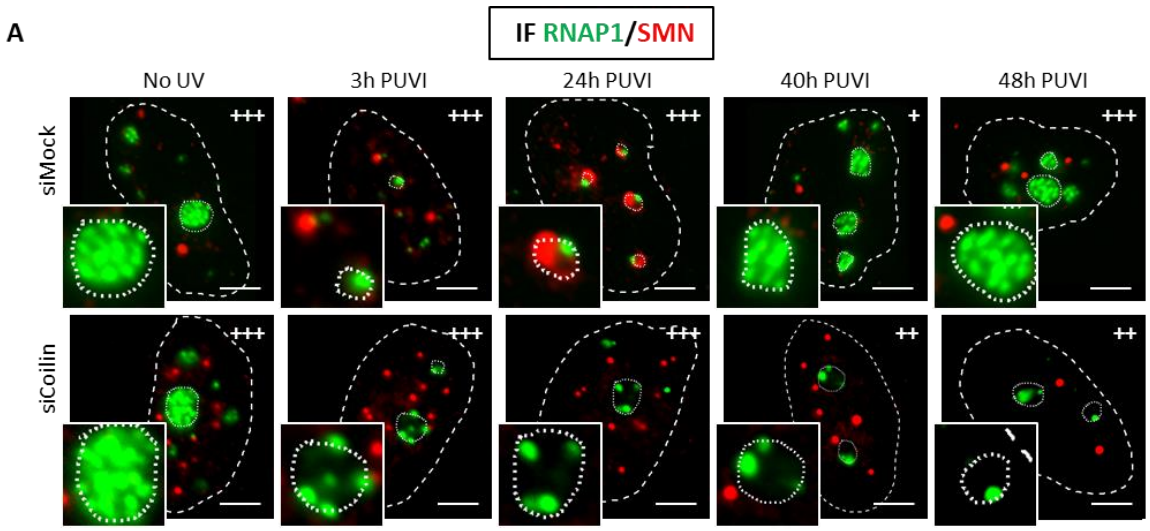
A
IF RNAP1/SMN
No UV
3h PUVI
24h PUVI
40h PUVI
48h PUVI
siMock
siCoilin
+++
+
++

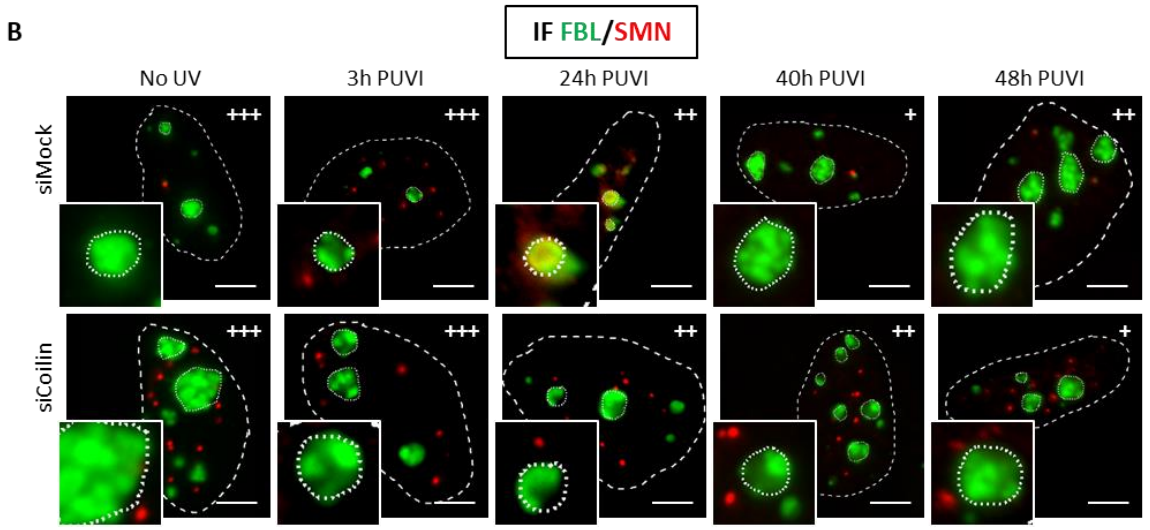
B
IF FBL/SMN
No UV
3h PUVI
24h PUVI
40h PUVI
48h PUVI
siMock
siCoilin
+++
++
+

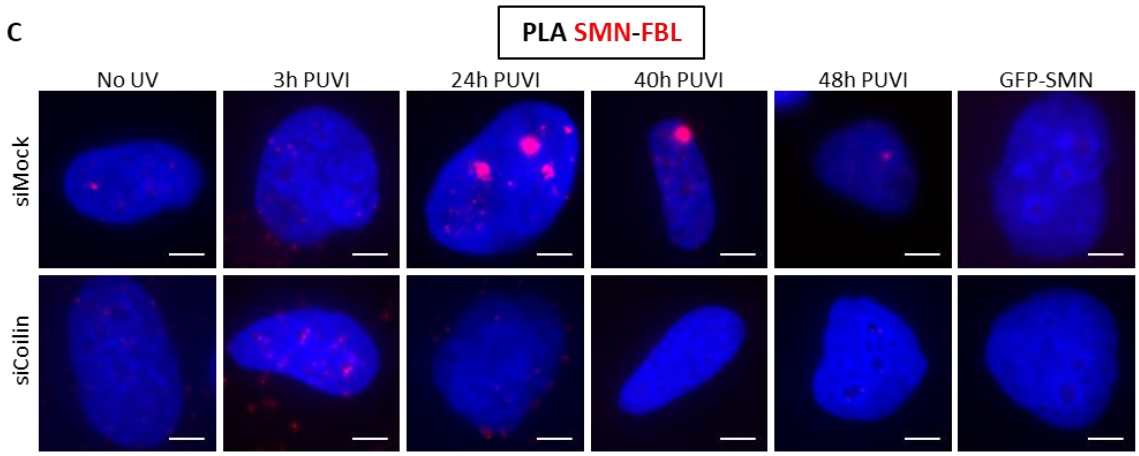
C
PLA SMN-FBL
No UV
3h PUVI
24h PUVI
40h PUVI
48h PUVI
GFP-SMN
siMock
siCoilin

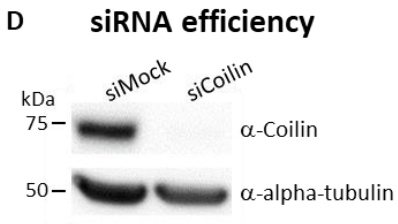
D
siRNA efficiency
siMock
siCoilin
kDa
75
50
α-Coilin
α-alpha-tubulin

264

Figure 4: SMN shuttling is Coilin-depdendent

(A and B) *Representative confocal microscopy images of IF in MRC5 cells transfected with siMock or siCoilin after 16J/m² UV-C irradiation showing the localization of SMN (red) and* ***(A)*** *RNAP1 or* ***(B)*** *FBL (green). Nuclei and nucleoli are indicated by dashed lines and dotted lines respectively. The number of the representative cells are indicated as followed + : 50–70%; ++ : 70–90%; +++ : >90%.* ***(C)*** *Representative microscopy images of PLA showing the interaction between SMN and FBL in MRC5 cells transfected with siMock or siCoilin after UV-C irradiation. Scale bar for all images: 5µm.* ***(D)*** *Western Blot on whole cell extracts of MRC5 cells treated with siCoilin.*

FBL is required for SMN export from the nucleolus and for the nucleolar rearrangement following UV-C exposure.

As Coilin, FBL is an essential partner of SMN and a nucleolar protein that can methylate rDNAs and Histones within the nucleolus [19,22]. We showed that FBL and SMN interact in cell extracts by GST (Figure S3C and 3A) and *in vivo* by PLA (Figure 3B), notably stronger after SMN shuttling into the nucleolus (24h PUVI). As the SMN shuttling is dependent on Coilin (Figure 4), we wondered whether FBL depletion would play a role in this shuttling process. To test this hypothesis, we depleted cells of FBL by using a specific siRNA (Figure 5D) and performed IF of SMN and RNAP1 on wild-type cells before damage and at different time PUVI (Figure 5A) in presence or absence of FBL. Our results show that without FBL, the shuttling of SMN within the nucleolus is altered, namely SMN is localized at the periphery of the nucleolus already at 3h PUVI and stays at the periphery of the nucleolus at all time points, without entering the nucleolus (Figure 5A). Importantly, in cells deficient for FBL, the nucleolar reorganization after DNA damage and repair is not repristinated and RNAP1 remains at the periphery of the nucleolus at 48h PUVI, indicating that the shuttling of SMN within the nucleolus and the presence of FBL are both important to insure the reestablishment of the nucleolar reorganization. Interestingly, in the absence of FBL, some colocalization between RNAP1 and SMN can be observed (Figure 5A).

To verify if and how the absence of FBL affects the interaction between SMN and Coilin, we performed PLA and IF of SMN and Coilin on wild-type cells before damage and at different time PUVI (Figure 5B and 5C) in presence or absence of FBL. Our results show that, without FBL, the interaction between SMN and Coilin is detectable at all times PUVI (Figure 5C) and both SMN and Coilin are localized at the periphery of the nucleolus already at 3h PUVI, this localization does not change at 24h or 40h PUVI (Figure 5B). These findings show that FBL is also a critical player in SMN shuttling and in appropriate nucleolar reorganization following UV irradiation and DNA repair.

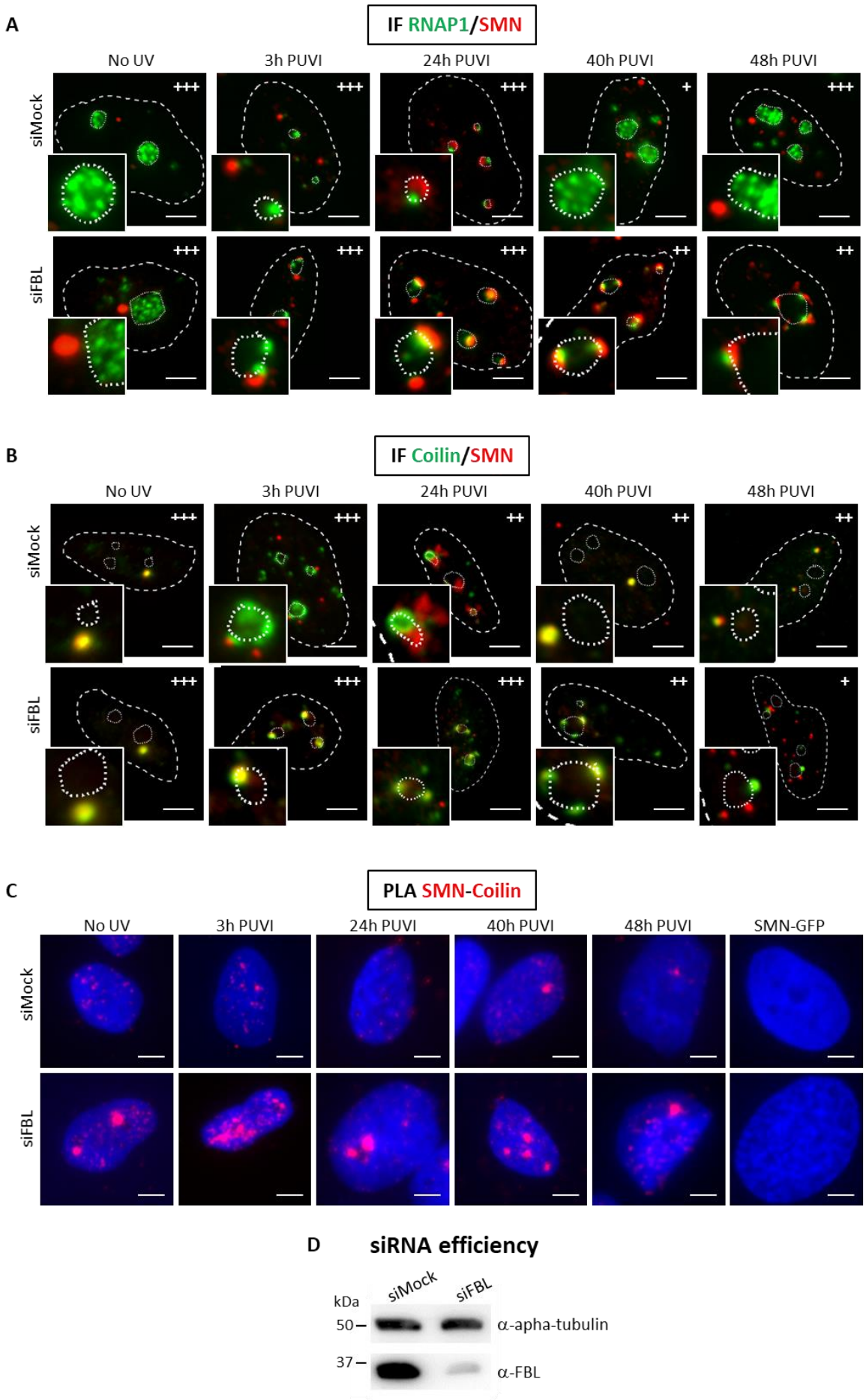
A
IF RNAP1/SMN
No UV
3h PUVI
24h PUVI
40h PUVI
48h PUVI
siMock
siFBL
B
IF Coilin/SMN
C
PLA SMN-Coilin
SMN-GFP
D
siRNA efficiency
kDa
50
37
α-apha-tubulin
α-FBL

297

Figure 5: The release of SMN into the nucleolus is FBL-dependent

(A and B) *Representative confocal microscopy images of IF in MRC5 cells transfected with siMock or siFBL after 16J/m² UV-C irradiation showing the localization of SMN (red) and* ***(A)*** *RNAP1 or* ***(B)*** *Coilin (green). Nuclei and nucleoli are indicated by dashed lines and dotted lines respectively. The number of the representative cells are indicated as followed + : 50–70%; ++ : 70–90%; +++ : >90%.* ***(C)*** *Representative microscopy images of PLA showing the interaction between Coilin and SMN in MRC5 cells transfected with siMock or siFBL after UV-C irradiation. Scale bar for all images: 5µm.* ***(D)*** *Western Blot on whole cell extracts of MRC5 cells treated with siFBL.*

PRMT1 activity mediates the nucleolar shuttling of SMN

One of the activities of SMN is to bind, via the Tudor domain, Arginine methylated proteins [23,24]. Arginine methylation is a widespread post-translational modification that can occur in histones and non-histone proteins [25–28]. The enzymes catalyzing the transfer of a methyl group to Arginine residues are part of a family called the PRMTs (Protein Arginine Methyl Transferases). PRMTs can mono-methylate Arginine residues (MMA) or di-methylate Arginine residues either symmetrically (SDMA) or asymmetrically (ADMA). Because these proteins affect SMN functions but also the interaction of SMN with Coilin [29], we wondered whether one of the PRMTs could affect, disturb or enhance SMN shuttling after DNA damage. Using GST pull-down assay, we observed that PRMT1 interact with SMN (Figure S5A). We thus decided to deplete cells from PRMT1 by siRNA silencing (Figure 6D) and performed IF against SMN and FBL. We found that PRMT1 inhibited the entry of SMN within the nucleolus at 24h PUVI (Figure 6A). In fact, in PRMT1 depleted cells, SMN reaches the periphery of the nucleolus already at 3h PUVI but remains at the periphery and cannot enter the nucleolus at later time points. This SMN localization after DNA damage is reminiscent of the one observed in FBL depleted cells (Figure 5A). To investigate how the depletion of PRMT1 affects the interactions between SMN and its partners (Coilin and FBL), we performed PLA assays and measured a stronger interaction of SMN and FBL specifically at 3h PUVI which correlates with the localization of SMN at the periphery of the nucleolus at this precise time point (Figure 6B). We also quantified a stronger interaction of SMN with Coilin when PRMT1 is depleted (Figure 6C) before damage induction and up to 40h PUVI. PRMT1 is part of the class I PRMTs which perform ADMA and MMA, in this class other PRMTs are found (PRMT-3 -4 -6 and -8).

To verify whether the perturbation of SMN shuttling observed in Figure 6A is due to the physical depletion of PRMT1 or the inhibition of the ADMA methylase activity, we treated the cells with the PRMT-class I specific inhibitor MS023 [30] (Figure 7A and S5B) prior to DNA damage and IF assays. We could verify that the inhibition of the methylase activity of PRMTs from class I is perturbing SMN shuttling (Figure 7A and S5B) and that SMN is unable to enter the nucleolus at 24h PUVI and is localized at the

periphery of the nucleolus already at 3h PUVI, a situation that is reminiscent of both FBL depletion (Figure 5A) and PRMT1 depletion (Figure 6A). Interestingly, by using the more specific and potent PRMT1 inhibitor, Furamidine[31], we could observe a complete abolishment of SMN shuttling at all time points (Figure 7A and S5B).

Remarkably, we showed by IF that PRMT1 is also shuttling during nucleolar reorganization in wild type cells and could detect PRMT1 at 24h and 40h PUVI (in a subset of cells) within the nucleolus (Figure 7B). Moreover, at late time points, when SMN localization within the CBs is restored, PRMT1 is no more localized in the nucleolus and surprisingly PRMT1 levels increase in the nucleoplasm (Figure 7B). Importantly, the shuttling of PRMT1 within the nucleolus is dependent on the SMN protein as in SMN depleted cells (Sh6-SMN), PRMT1 is not detected inside the nucleoli at 24h and 40h PUVI (Figure 7B). However, the nuclear increase of PRMT1 level is independent of the presence of a functional SMN.

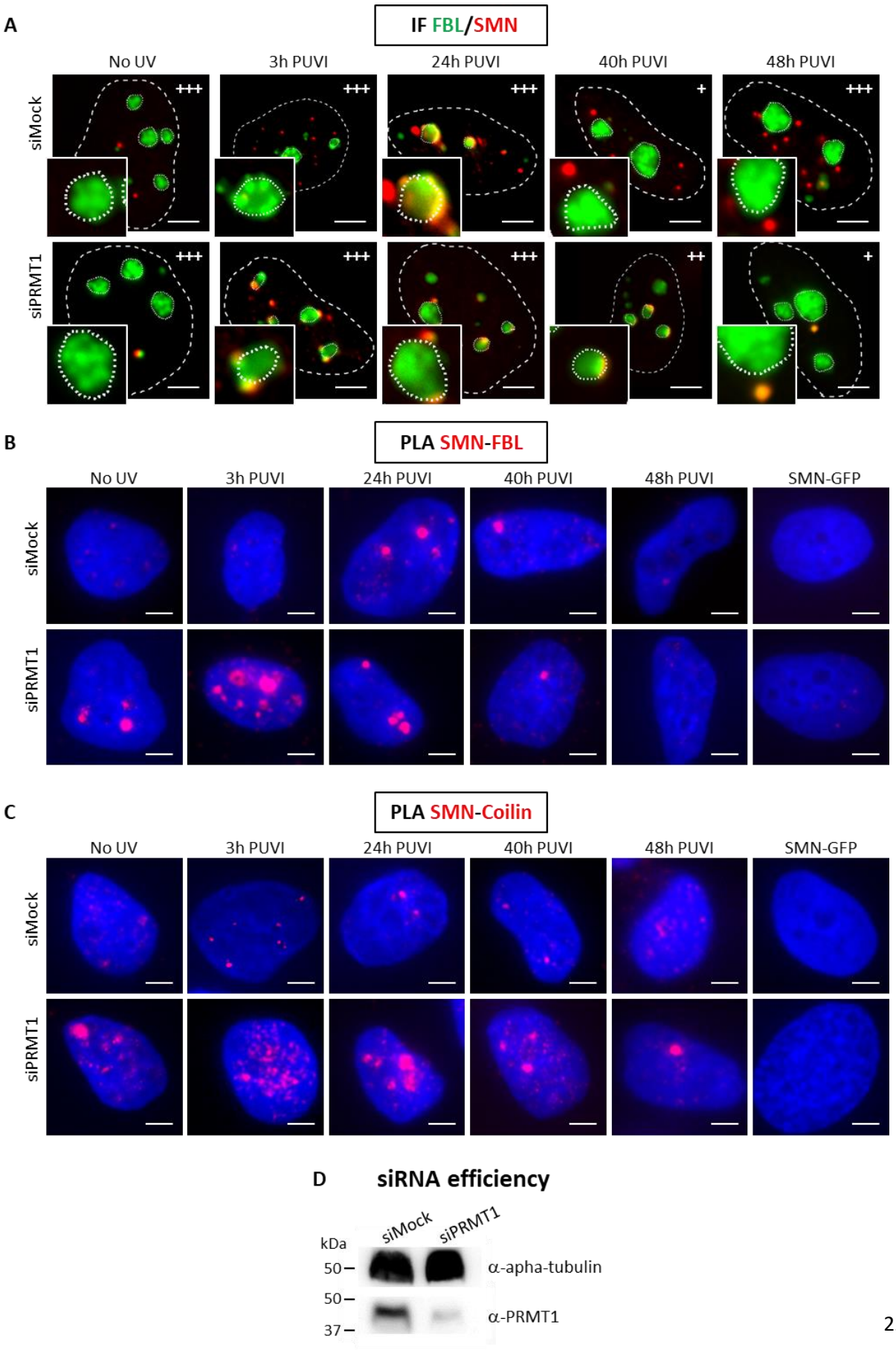
A
IF FBL/SMN
No UV
3h PUVI
24h PUVI
40h PUVI
48h PUVI
siMock
siPRMT1
+++
+
++
B
PLA SMN-FBL
SMN-GFP
C
PLA SMN-Coilin
D
siRNA efficiency
kDa
siMock
siPRMT1
50
37
α-apha-tubulin
α-PRMT1

343

Figure 6: PRMT1 remodel the interaction of SMN with FBL and Coilin

(A) *Representative confocal microscopy images of IF in MRC5 cells transfected with siMock or siPRMT1 after 16J/m² UV-C irradiation showing the localization of SMN (red) and FBL (green). Nuclei and nucleoli are indicated by dashed lines and dotted lines respectively. The number of the representative cells are indicated as followed + : 50–70%; ++ : 70–90%; +++ : >90%.* ***(B and C)*** *Representative microscopy images of PLA showing the interaction between SMN and FBL* ***(B)*** *and between SMN and Coilin* ***(C)*** *in MRC5 cells transfected with siMock or siPRMT1 after UV-C irradiation. Scale bar for all images: 5µm.* ***(D)*** *Western Blot on whole cell extracts of MRC5 cells treated with siPRMT1.*

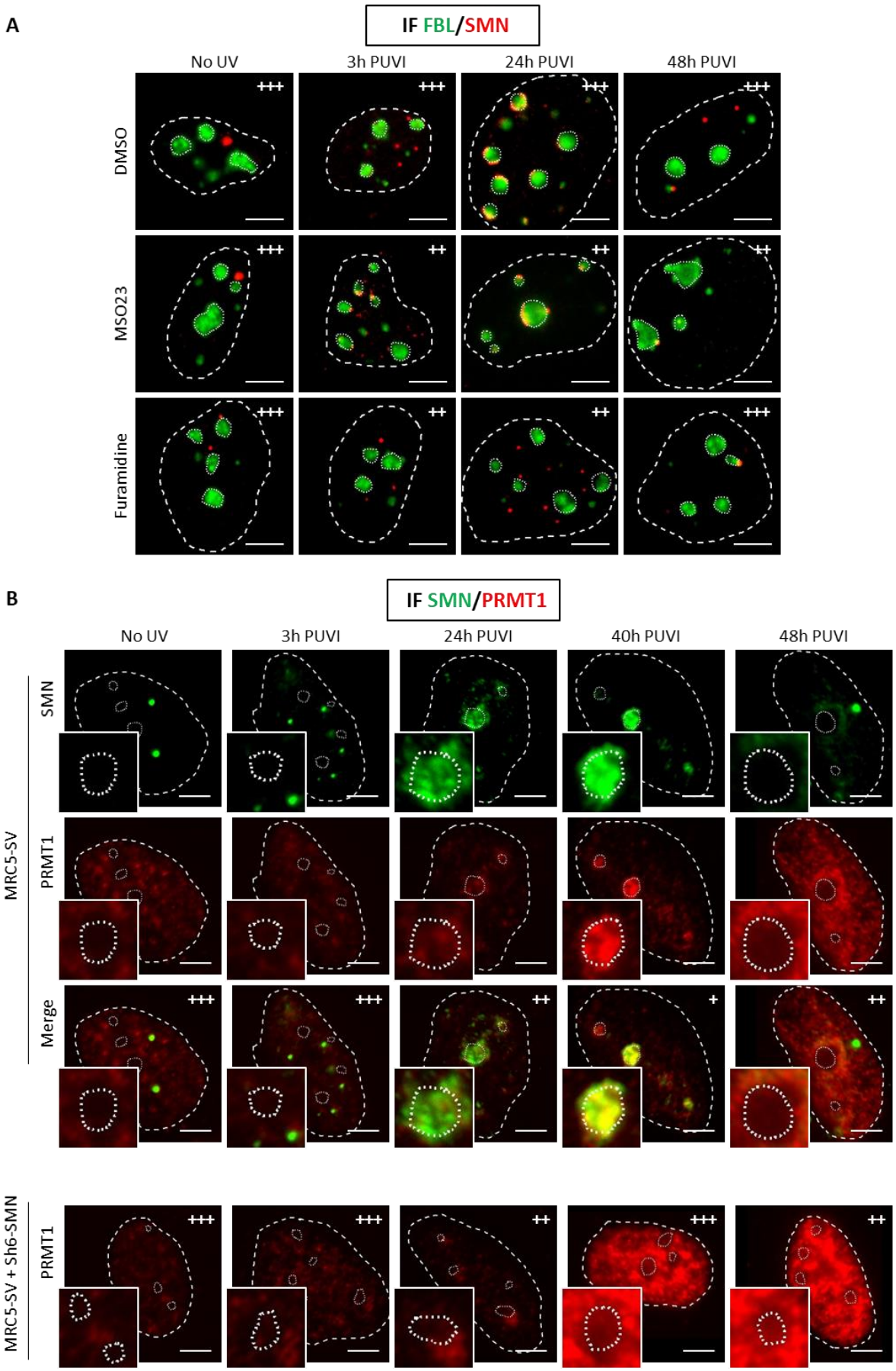
A
IF FBL/SMN
No UV
3h PUVI
24h PUVI
48h PUVI
DMSO
MSO23
Furamidine
+++
++
B
IF SMN/PRMT1
No UV
3h PUVI
24h PUVI
40h PUVI
48h PUVI
MRC5-SV
SMN
PRMT1
Merge
+
MRC5-SV + Sh6-SMN
PRMT1

Figure 7: PRMT1 activity mediates the nucleolar shuttling of SMN.

(A) *Representative confocal microscopy images of IF in MRC5 cells treated with DMSO, MS023 or Furamidine followed by 16J/m² UV-C irradiation showing the localization of SMN (red) and FBL (green).* ***(B)*** *Representative microscopy images of IF in MRC5 and Sh6-SMN cells after 16J/m² UV-C irradiation showing the localization of SMN (green) and PRMT1 (red). Nuclei and nucleoli are indicated by dashed lines and dotted lines respectively. Scale bar for all images: 5µm. The number of the representative cells are indicated as followed + : 50–70%; ++ : 70–90%; +++ : >90%.*

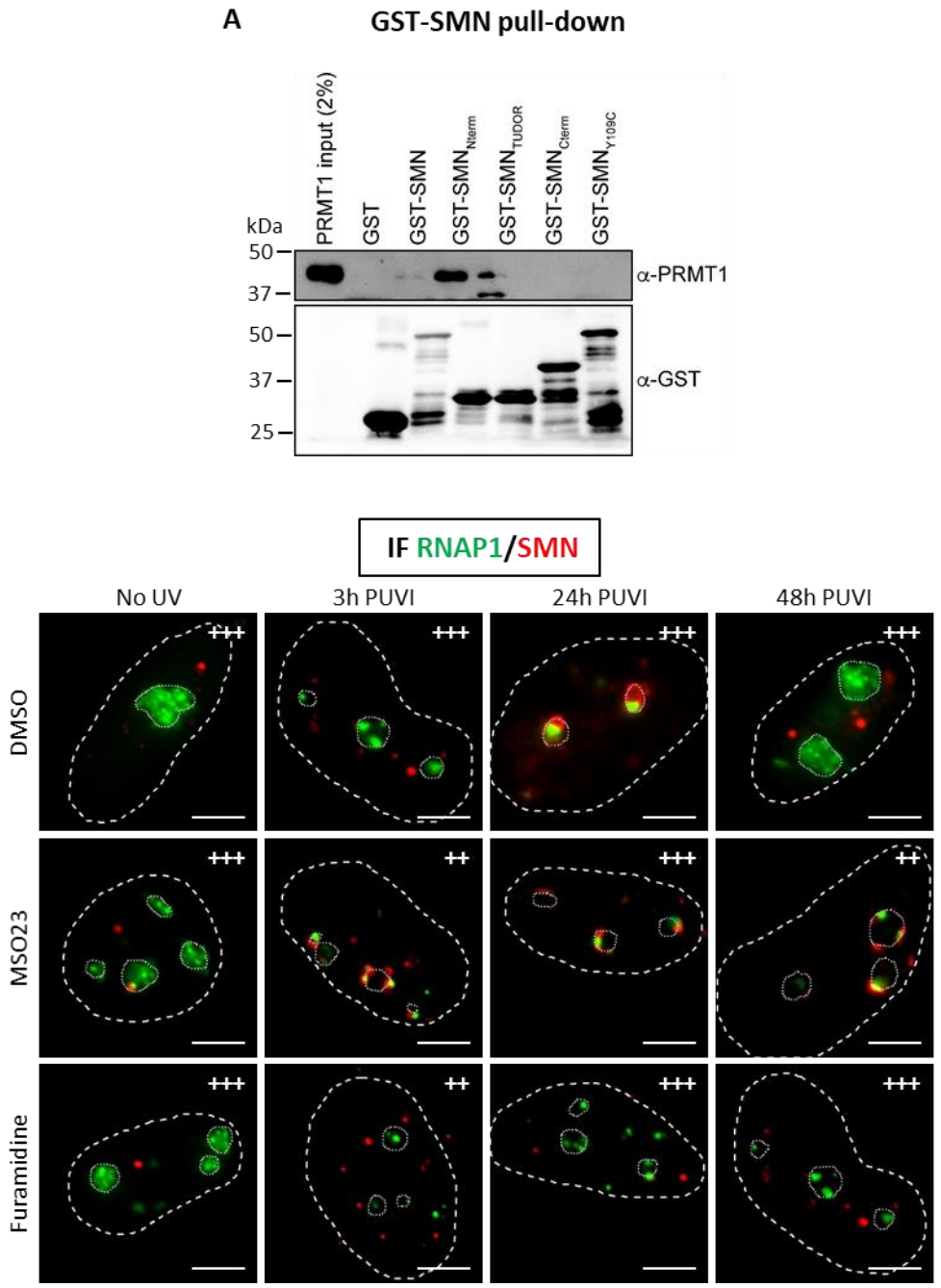

Figure S5: Relation between PRMT1 and SMN.

(A) *GST pull-down assay using purified recombinant SMN protein with different truncation of the protein and cellular extracts.* ***(B)*** *Representative confocal microscopy images of IF in MRC5 cells treated with DMSO, MS023 or Furamidine followed by 16J/m² UV-C irradiation showing the localization of SMN (red) and RNAP1 (green). Nuclei and nucleoli are indicated by dashed lines and dotted lines respectively. Scale bar for all images: 5µm. The number of the representative cells are indicated as followed + : 50–70%; ++ : 70–90%; +++ : >90%.*

DISCUSSION

One of the most fascinating and nearly unexplored area in the DNA repair field is how cells repristinate their cellular activities after the completion of all the reactions that allow cells to eliminate DNA lesions. Most DNA lesions block transcription and replication [5] and although we have an extensive knowledge on how cells recognize and repair DNA lesions, very little is known on how cells restart these cellular processes. In post-mitotic cells, restoration of the damage-induced block of transcription is essential for cell survival.

We have shown that RNAP1 transcription is blocked after UV lesions and that TC-NER pathway is responsible for the repair of UV-lesions on ribosomal DNA [7]. Importantly, UV-damages impact the organization of the nucleolus and during DNA repair both nucleolar DNA and RNAP1 are displaced at the periphery of the nucleolus [7]. Interestingly, although RNAP1 transcription restarts when UV-lesions on the transcribed strand are repaired, the positioning of the RNAP1 within the nucleolus is dependent on the presence of DNA lesions on the untranscribed nucleolar DNA [7]. In this particular case, RNAP1 transcription restarts in a non-canonical compartment and this anomaly might influence the proper ribosome biogenesis. Therefore, the restoration of the proper nucleolar structure and organization might be important for the cellular viability or for the efficiency of cellular processes. The recovery of a normal nucleolar structure is not a passive process and require the presence of some key proteins [8], although their exact mechanistic role have not been established yet.

In a quest of finding the exact molecular mechanism for the reestablishment of the nucleolar organization after DNA repair completion, we set up a best candidate approach that guided us to inspect the effect of depletion of different nucleolar proteins' interactors. One of these candidates was the protein SMN, which is a particularly interesting protein to scrutinize because of the known interaction with the nucleolar protein FBL via its Tudor domain [16]. We demonstrate in this study that silencing or mutation of the SMN protein impedes RNAP1 and FBL to recover the proper position within the nucleolus after DNA repair, despite the restart of RNAP1 transcription (Figure 1). To note, this mis-localization is not induced by the presence of DNA lesions because SMN deficient cells are proficient in the NER pathway, repairing UV-lesions on both transcribed and untranscribed regions of the genome (Figure S2).

Interestingly, we have observed that SMN, together with Gemin5, protein belonging to the SMN complex, shuttles within the nucleolus, prior the reestablishment of the proper nucleolar landscape (Figure 2D). Indeed, in normal wild type cells, after UV irradiation (or RNAP1 transcription inhibition), the CBs are disrupted [21] and Coilin is displaced to the periphery of the nucleolus (Figure 2C). At later time points, likely when DNA repair is mostly completed, SMN (and Gemin5) reaches the periphery of the nucleolus and is localized within the nucleolus (Figure 2A and 2B). Finally, when cells that have reestablished the

proper localization of RNAP1/FBL within the nucleolus, SMN and Coilin are found in their physiological localization within the CBs.

The different phases of SMN shuttling are dependent on both Coilin and FBL (Figure 4 and 5). In Coilin depleted cells, SMN does not reach the periphery of the nucleolus and in FBL depleted cells, SMN does not enter the nucleolus, remaining at its periphery. In both Coilin and FBL depleted cells, RNAP1 does not recover the proper localization within the nucleolus but remains at the periphery of the nucleolus. Because FBL interacts with SMN via its Tudor domain [16] (Figure S3) and SMN interacts mainly with methylated Arginines residues, we explored the possibility that one of the PRMTs would be responsible for SMN shuttling within the nucleolus. Indeed, the activity of PRMT1, responsible for ADMA, is essential to recruit SMN to the periphery of and within the nucleolus (Figure 6). Interestingly, PRMT1 also shuttles within the nucleolus and at the same time after irradiation as SMN (Figure 7). Remarkably, this shuttling is SMN dependent. Although we do not know if the substrate of PRMT1 is a protein that directly interact with SMN, we showed that methylation is essential for SMN shuttling. It is plausible to assume that because FBL is methylated by PRMT1 [32], FBL might be the substrate methylated during the process of RNAP1 repositioning within the nucleolus after completion of DNA repair.

Our results show a newly discovered SMN function in nucleolar homeostasis and may directly impact the life and well-being of SMA patients [33]. In fact, in cells and motoneurons of SMA patients, exogenous and endogenous DNA damage might progressively and lastingly disrupt nucleolar structure and disturb ribosome biogenesis leading to perturbed protein translation [34]. This defect may contribute to the neurodegenerative phenotype of SMA motoneurons. If this hypothesis is true, SMA patients could be advised to prevent deleterious DNA damage to avoid a reorganization of the nucleolus that would affect proper protein production within neurons.

Although exogeneous DNA damage is partially avoidable, endogenous DNA damage is inevitable and one way to reduce its overload is to follow a diet rich in anti-oxidants. This nutritional approach combined with a healthy lifestyle, avoiding exogenous damage, such as cigarette smoke, pollutants, and potentially harmful molecules, may retard the degeneration of motoneurons and thus SMA progression.

MATERIALS AND METHODS

Cell culture and treatments

SV40-immortalized human fibroblasts, wild-type (MRC5-SV) and CSB-deficient (CS1AN-SV), were cultured in DMEM supplemented with 10% fetal bovine serum (FBS) and 1% penicillin and streptomycin (P/S) and incubated at 37°C with 20% O2 and 5% CO2.

The MRC5-SV + Sh cells were obtained by transduction of lentiviral particles produced (as described https://www.addgene.org/protocols/plko/#Ehttps://www.addgene.org/protocols/plko/ - E) from piSMART hEF1α/turboGFP (Dharmacon) doxycycline-inducible lentiviral system containing a Short Hairpin (Sh) Scramble (VSC6572), Sh5-SMN (V3IHSHEG_4923340; mature antisense: TAAACTACAACACCCTTCT) or Sh6-SMN (V3IHSHEG_5297527; mature antisense: TTCAAATTTTCTCAACTGC). ShSMN both target telomeric *SMN1* and centromeric *SMN2* copies of the gene. The cells were cultured in DMEM supplemented with 10% FBS and 1% P/S; maintained in 100 ng/ml puromycin. Sh expression is induced with 100 ng/ml doxycycline. The cells were incubated at 37°C with 20% O_2 and 5% CO_2.

Primary fibroblast cells from unaffected (C5RO) and CSB-deficient patients (CS1AN) were cultured in DMEM supplemented with 10% FBS and 1% P/S. SMA type I patients (GM00232) fibroblast cell lines were obtained from Coriell Cell Repositories and cultured in MEM supplemented with 15% non-inactivated FBS, 1% non-essential amino acids and 1% P/S. All primary fibroblasts are incubated at 37°C with 3% O2 and 5% CO2.

DNA damage was inflicted by UV-C light (254 nm, 6-Watt lamp). Cells were globally irradiated with a UV-C dose of 16 J/m² or locally irradiated with a UV-C dose of 100 J/m² through a filter with holes of 5µm. After irradiation, cells were incubated at 37°C with 5% CO2 for different periods of time.

The PRMT inhibitor, MS023 (ab223596) diluted in DMSO, was added at 1µM in the medium 20h before irradiation. The PRMT1 inhibitor, Furamidine (ab287098) diluted in DMSO, was added at 1µM in the medium 15h before irradiation

Transfection of small interfering RNAs (siRNAs)

Cells were seeded in six-well plates with coverslip and allowed to attach. Cells were transfected two times in an interval of 24h with siRNA using Lipofectamine® RNAiMAX reagent (Invitrogen; 13778150) according to the manufacturer' protocol. Experiments were performed between 24h and 72h after the second transfection. Protein knock-down was confirmed for each experiment by western blot. The small interfering RNA (siRNAs) used in this study are: siMock, Horizon, D-001206-14 (10nM); siCoilin, Horizon, M-019894-01 (5nM); siFBL, Horizon, L-011269-00 (10nM); siPRMT1, Horizon, L-010102-00

(10nM). The final concentration used for each siRNA is indicated in parentheses. All siRNA are a pool of four different siRNA.

Protein extraction

To verify siRNA efficiency, the coverslip need for the experiment was displaced before fixation and cells that remained in the dish were collected. The extraction of total proteins was performed using the PIERCE RIPA buffer (Thermo, #89900) complemented with EDTA-free cOmplete PIC (ROCHE).

GST-SMN purification and GST pull-downs

SMN (full-length or truncated) cDNA was cloned in pGEX6P1 between *BamHI* and *XhoI* sites and transformed in BL21 (DE3) cells (200131; Agilent). Single colonies were grown overnight in 2.5 mL LB broth, scaled up to 250 mL, grown at 37 °C until density at OD_{600} reached 0.6, then GST or GST-SMN were induced with 0.2 mM IPTG overnight. The next day, cells were collected by centrifugation and resuspended in 10 mL lysis buffer (50mM Tris pH 8.0, 150mM NaCl, 0.05% NP40, supplemented with PIC). While working on ice, cells were briefly sonicated and extracts clarified by centrifugation. Recombinant proteins were then purified using Glutathione-sepharose beads (thumbling at 4 °C overnight), washed extensively with lysis buffer, and released from the beads using elution buffer (100mM Tris pH 8.0, 10% Glycerol, 15mg/mL reduced glutathione).

GST pull-downs were performed in 600 µL TAP buffer (50mM Tris pH 7.5, 200mM NaCl, 0.1% Triton-X100, and 10% glycerol supplemented with PIC) with 5µg GST and 85µL HEK293T whole cell lysate (1 x 100 mm plate lysed in 1 mL TAP buffer). A 10% input (8.5µL in 20µL Laemmli sample buffer) was set aside. Samples were incubated 2-3h at 4°C with rotation, then 25µL Glutathione-sepharose beads were added for 1h. Finally, the beads were washed 4 times with 1mL TAP buffer and finally resuspended in 20µL Laemmli sample buffer before immunoblotting analyses.

For time course experiments following UV-induced DNA damage, MRC5-SV cells were lysed in Pierce IP lysis buffer (Thermo 87787) and 17µg of proteins (amount available per pull-down) were used as above.

Western blot

Proteins were separated on a SDS-PAGE gel composed of bisacrylamide (37:5:1), and then transferred onto a polyvinylidene difluoride membrane (PVDF, 0.45 µm; Millipore). The membrane was blocked in PBS-T (PBS and 0.1 % Tween 20) with 5 % milk and incubated for 2h at room temperature (RT) or overnight at 4°C with the primary antibodies diluted in milk PBS-T (see table of antibody). Subsequently, the membrane was washed with PBS-T (3× 5-10 min) and incubated with the following secondary antibody diluted 1/5000 in milk PBS-T: Goat anti-rabbit IgG HRP conjugate (170-6515; BioRad) or Goat anti-mouse IgG HRP conjugate (170-6516; BioRad). After the same washing procedure, protein bands were visualized

via chemiluminescence (ECL Enhanced Chemo Luminescence; Pierce ECL Western Blotting Substrate) using the ChemiDoc MP system (BioRad).

Cytostripping

To improve the nuclear signal of SMN, the cytoplasm of the cells was removed before fixation. After two washes with cold PBS, cells were incubated on ice 5 min with cold cytoskeleton buffer (10mM PIPES pH6,8; 100mM NaCl; 300mM Sucrose; 3mM MgCl2; 1mM EGTA; 0,5% Triton-X100) followed by 5min with cold cytostripping buffer (10mM Tris HCL pH7,4; 10mM NaCl; 3mM MgCl2; 1% Tween 40; 0,5% sodium deoxycholate). After three gentle washes with cold PBS, cells were fixed.

Immunofluorescence

Cells were grown on coverslips, washed with PBS at RT, and fixed with 2% paraformaldehyde (PFA) for 15min at 37° C. Cells were permeabilized with PBS 0.1 % Triton X-100 (3X short + 2X 10 min washes). Blocking of non-specific signals was performed with PBS+ (PBS, 0.5 % BSA, 0.15 % glycine) for at least 30 min. Then, coverslips were incubated with primary antibody diluted in PBS+ for 2h at room temperature (RT) or overnight at 4°C in a moist chamber. After several washes with PBS + 0.1% Triton X-100 (3X short + 2X 10 min) and a quick washed with PBS+, cells were incubated for 1h at RT in a moist chamber with the following secondary antibody coupled to fluorochrome and diluted 1/400 in PBS+ : Goat anti-mouse Alexa Fluor® 488 [A11001, Invitrogen] or 594 [A11005] and Goat anti-rabbit Alexa Fluor® 488 [A11008] or 594 [A11012]. After the same washing procedure but with PBS, coverslips were finally mounted using Vectashield with DAPI (Vector Laboratories).

Proximity ligation assay

PLA experiments were done using Duolink™ II secondary antibodies and detection kits (Sigma-Aldrich, #DUO92002, #DUO92004, and #DUO92008) according to the manufacturer's instructions. In brief, cells were fixed and permeabilized with the same procedure as immunofluorescence followed by incubation in PLA blocking buffer for 1h at 37 °C. After blocking, cells were incubated overnight at 4°C with primary antibodies diluted in PLA Antibody Diluent. After washes with PLA buffer A (1 short + 3x5min), cells were incubated with PLUS and MINUS PLA probes for 1h at 37 °C. After the same washing procedures with PLA buffer A, if probes were in close proximity (<40 nm), they were ligated together to make a closed circle thanks to the incubation of 30min at 37°C with the Duolink™ ligation solution. Then, after the same washing procedures, the DNA is amplified and detected by fluorescence 594 thanks to the incubation of 100min at 37°C with the Duolink™ amplification solution. After washing with PLA buffer B (1 short + 2x10min), coverslips were mounted using Vectashield with DAPI (Vector Laboratories).

Recovery of RNA synthesis (RRS) assay

Cells were grown on coverslips. RNA detection was done using a Click-iT RNA Alexa Fluor Imaging kit (Invitrogen, C10330), according to the manufacturer's instructions. Briefly, cells were UV-C irradiated (10 J/m²) and incubated for 3 or 24 h at 37°C. Then, cells were incubated for 2 hours with 5-ethynyl uridine (EU). After fixation and permeabilization, cells were incubated for 30min with the Click-iT reaction cocktail containing Alexa Fluor Azide 594. After washing, the coverslips were mounted with Vectashield (Vector). The average fluorescence intensity per nucleus was estimated after background subtraction using ImageJ and normalized to not treated cells. At least 50 cells were images for each condition of each cell lines.

RNA Fluorescence In Situ Hybridization (RNA-FISH)

Cells were grown on coverslips and globally irradiated for different times. Then, cells were washed with PBS at RT, and fixed with 4% PFA for 15min at 37° C. After two washes with PBS, cells were permeabilized with PBS+ 0.4 % Triton X-100 for 7min at 4° C. Cells were washed rapidly with PBS before incubation for at least 30min with pre-hybridization buffer (15% formamide in 2X SSPE pH8.0 [0.3M NaCl, 15.7mM $NaH_2PO_4.H_2O$ and 2.5mM EDTA]). 35ng of probe was diluted in 70µl of hybridization mix (2X SSPE, 15% formamide, 10% dextran sulfate and 0.5mg/ml tRNA). Hybridization of the probe was conducted overnight at 37°C in a humidified environment. Subsequently, cells were washed twice for 20 min with prehybridization buffer, then once for 20 min with 1X SSPE. After extensive washing with PBS, the coverslips were mounted with Vectashield containing DAPI (Vector Laboratories). The probe sequence (5' to 3') is Cy5- AGACGAGAACGCCTGACACGCACGGCAC. At least 30 cells were imaged for each condition of each cell lines.

Unscheduled DNA synthesis (UDS or TCR-UDS).

Cells were grown on coverslips. After local irradiation, cells were incubated for 3 or 8 hours (UDS and TCR-UDS respectively) with 20µM of 5-ethynyl-2'-deoxyuridine (EdU), fixed with 4% PFA for 15min at 37°C and permeabilized with PBS and 0.5% Triton X-100 for 20min. Then, cells were blocked with PBS+ for 30min and subsequently incubated for 1h at RT with mouse monoclonal anti-yH2AX antibody (Ser139 [Upstate, clone JBW301]) 1:500 diluted in PBS+. After extensive washes with PBS containing 0.5% Triton X100, cells were incubated for 45min at RT with secondary antibodies conjugated with Alexa Fluor 594. Next, cells were washed several times and then incubated for 30 min with the Click-iT reaction cocktail containing Alexa Fluor Azide 488 (Invitrogen, C10337). After washing, the coverslips were mounted with Vectashield containing DAPI (Vector). Images of the cells were obtained with the same microscopy system and constant acquisition parameters.

Images were analyzed as follows using ImageJ and a circle of constant size for all images: (i) the background signal was estimated in the nucleus (avoiding the damage, nucleoli and other non-specific

signal) and subtracted, (ii) the locally damaged area was defined by using the yH2AX staining, (iii) the average fluorescence correlated to the EdU incorporation was then measured and thus an estimate of DNA synthesis after repair was obtained.

Primary Antibodies

The following primary antibodies were used:

Antibody against	Manufacturer	Catalog Nr	Source	IF/PLA	WB
Alpha-Tubulin	Sigma	T6074	Mouse		1/50 000
Coilin	Proteintech	10967-1-AP	Rabbit	1/500	1/5000
CSB	Santa Cruz Biotechnology	sc398022	Mouse		1/100
FBL	abcam	ab5821	Rabbit	1/500	1/500
GST	abcam	ab3416	Rabbit		1/3000
PRMT1	Abcam	ab190892	Rabbit	1/5000	1/1000
RNAP1	Santa-cruz	sc48385	Mouse	1/500	
SMN	Proteintech	11708-1-AP	Rabbit	1/100	
SMN	BD Biosciences	610646	Mouse	1/500	1/5000

Images acquisition and analysis

Confocal images of the cells were obtained using a Zeiss LSM 780 NLO confocal laser scanning microscope and the following objective: Plan-Apochromat 63X/1.4 oil DIC M27 or 40X/1.3 oil DIC. The acquisition software is ZEN. Other images were obtained using Zeiss Z1 imager right with a 40x/0.75 dry objective. The acquisition software is Metavue.

Images of the cells for each experiment were obtained with the same microscopy system and constant acquisition parameters. Images were analyzed with Image J software. For all images of this study, nuclei and nucleoli were delimited with dashed and dotted lines respectively, using DAPI staining. ll experiments have been performed at least two times and are biological replicates.

Error bars represent the Standard Error of the Mean (SEM) of the biological replicates. Excel was used for statistical analysis and plotting of all the numerical data. Statistics were performed using a Student's test to compare two different conditions (siMock vs. siRNA X or No UV irradiation vs. after irradiation) with the following parameters: two-tailed distribution and two-sample unequal variance (heteroscedastic).

Acknowledgments

We would like to thank Dr Leonardo Beccari for fruitful discussions and Dr Laurent Schaeffer for supporting and encouraging this research. We are grateful to the imaging platform CIQLE and Dr Christophe Vanbel together with the CRCL imaging facility.

Conflicts of interest

The authors disclose no potential conflict of interest.

Funding

This work was supported by AFM-Téléthon (MyoNeurALP 1 and 2) and by Institut National du Cancer (InCa, PLBIO19-126).

SM was funded by Jazan university, Jazan, Saudi Arabia.

PL and OB are funded by an AFM-Téléthon grant (MyoNeurALP) and by the Joint Collaborative Research Program between the Centre for Neuromuscular Disease (University of Ottawa) and Institut NeuroMyoGène (INMG - Claude Bernard Université Lyon 1).

JC is funded by a Canadian Institutes of Health Research (CIHR) grant (MOP 123381) and CureSMA Canada.

REFERENCES

1. Dubois, M.-L. & Boisvert, F.-M. The Nucleolus: Structure and Function. in *The Functional Nucleus* (eds. Bazett-Jones, D. P. & Dellaire, G.) 29–49 (Springer International Publishing, 2016). doi:10.1007/978-3-319-38882-3_2.
2. Hernandez-Verdun, D. Assembly and disassembly of the nucleolus during the cell cycle. *Nucl. Austin Tex* **2**, 189–194 (2011).
3. Boulon, S., Westman, B. J., Hutten, S., Boisvert, F.-M. & Lamond, A. I. The nucleolus under stress. *Mol. Cell* **40**, 216–227 (2010).
4. Louvet, E., Junéra, H. R., Le Panse, S. & Hernandez-Verdun, D. Dynamics and compartmentation of the nucleolar processing machinery. *Exp. Cell Res.* **304**, 457–470 (2005).
5. Giglia-Mari, G., Zotter, A. & Vermeulen, W. DNA damage response. *Cold Spring Harb. Perspect. Biol.* **3**, a000745 (2011).
6. Brooks, P. J. The case for 8,5'-cyclopurine-2'-deoxynucleosides as endogenous DNA lesions that cause neurodegeneration in xeroderma pigmentosum. *Neuroscience* **145**, 1407–1417 (2007).
7. Daniel, L. *et al.* Mechanistic insights in transcription-coupled nucleotide excision repair of ribosomal DNA. *Proc. Natl. Acad. Sci. U. S. A.* **115**, E6770–E6779 (2018).
8. Cerutti, E. *et al.* β-Actin and Nuclear Myosin I are responsible for nucleolar reorganization during DNA Repair. 646471 Preprint at https://doi.org/10.1101/646471 (2019).
9. Talbot, K. & Tizzano, E. F. The clinical landscape for SMA in a new therapeutic era. *Gene Ther.* **24**, 529–533 (2017).
10. Monani, U. R. Spinal muscular atrophy: a deficiency in a ubiquitous protein; a motor neuron-specific disease. *Neuron* **48**, 885–896 (2005).
11. Calucho, M. *et al.* Correlation between SMA type and SMN2 copy number revisited: An analysis of 625 unrelated Spanish patients and a compilation of 2834 reported cases. *Neuromuscul. Disord. NMD* **28**, 208–215 (2018).

12. Singh, R. N., Howell, M. D., Ottesen, E. W. & Singh, N. N. Diverse role of survival motor neuron protein. *Biochim. Biophys. Acta Gene Regul. Mech.* **1860**, 299–315 (2017).

13. Trinkle-Mulcahy, L. & Sleeman, J. E. The Cajal body and the nucleolus: 'In a relationship' or 'It's complicated'? *RNA Biol.* **14**, 739–751 (2017).

14. Hebert, M. D., Szymczyk, P. W., Shpargel, K. B. & Matera, A. G. Coilin forms the bridge between Cajal bodies and SMN, the spinal muscular atrophy protein. *Genes Dev.* **15**, 2720–2729 (2001).

15. Wehner, K. A. *et al.* Survival motor neuron protein in the nucleolus of mammalian neurons. *Brain Res.* **945**, 160–173 (2002).

16. Jones, K. W. *et al.* Direct interaction of the spinal muscular atrophy disease protein SMN with the small nucleolar RNA-associated protein fibrillarin. *J. Biol. Chem.* **276**, 38645–38651 (2001).

17. Renvoisé, B. *et al.* Distinct domains of the spinal muscular atrophy protein SMN are required for targeting to Cajal bodies in mammalian cells. *J. Cell Sci.* **119**, 680–692 (2006).

18. Thandapani, P., O'Connor, T. R., Bailey, T. L. & Richard, S. Defining the RGG/RG motif. *Mol. Cell* **50**, 613–623 (2013).

19. Pellizzoni, L., Baccon, J., Charroux, B. & Dreyfuss, G. The survival of motor neurons (SMN) protein interacts with the snoRNP proteins fibrillarin and GAR1. *Curr. Biol. CB* **11**, 1079–1088 (2001).

20. Whitehead, S. E. *et al.* Determinants of the Interaction of the Spinal Muscular Atrophy Disease Protein SMN with the Dimethylarginine-modified Box H/ACA Small Nucleolar Ribonucleoprotein GAR1 *. *J. Biol. Chem.* **277**, 48087–48093 (2002).

21. Cioce, M., Boulon, S., Matera, A. G. & Lamond, A. I. UV-induced fragmentation of Cajal bodies. *J. Cell Biol.* **175**, 401–413 (2006).

22. Tessarz, P. *et al.* Glutamine methylation in histone H2A is an RNA-polymerase-I-dedicated modification. *Nature* **505**, 564–568 (2014).

23. Friesen, W. J., Massenet, S., Paushkin, S., Wyce, A. & Dreyfuss, G. SMN, the product of the spinal muscular atrophy gene, binds preferentially to dimethylarginine-containing protein targets. *Mol. Cell* **7**, 1111–1117 (2001).

24. Sprangers, R., Groves, M. R., Sinning, I. & Sattler, M. High-resolution X-ray and NMR structures of the SMN Tudor domain: conformational variation in the binding site for symmetrically dimethylated arginine residues. *J. Mol. Biol.* **327**, 507–520 (2003).

25. Fulton, M. D., Brown, T. & Zheng, Y. G. Mechanisms and Inhibitors of Histone Arginine Methylation. *Chem. Rec. N. Y. N* **18**, 1792–1807 (2018).

26. Bedford, M. T. & Richard, S. Arginine methylation an emerging regulator of protein function. *Mol. Cell* **18**, 263–272 (2005).

27. Di Lorenzo, A. & Bedford, M. T. Histone arginine methylation. *FEBS Lett.* **585**, 2024–2031 (2011).

28. Lee, Y.-H. & Stallcup, M. R. Minireview: protein arginine methylation of nonhistone proteins in transcriptional regulation. *Mol. Endocrinol. Baltim. Md* **23**, 425–433 (2009).

29. Hebert, M. D., Shpargel, K. B., Ospina, J. K., Tucker, K. E. & Matera, A. G. Coilin methylation regulates nuclear body formation. *Dev. Cell* **3**, 329–337 (2002).

30. Eram, M. S. *et al.* A Potent, Selective, and Cell-Active Inhibitor of Human Type I Protein Arginine Methyltransferases. *ACS Chem. Biol.* **11**, 772–781 (2016).

31. Yan, L. *et al.* Diamidine compounds for selective inhibition of protein arginine methyltransferase 1. *J. Med. Chem.* **57**, 2611–2622 (2014).

32. Lin, C.-H., Huang, H.-M., Hsieh, M., Pollard, K. M. & Li, C. Arginine methylation of recombinant murine fibrillarin by protein arginine methyltransferase. *J. Protein Chem.* **21**, 447–453 (2002).

33. Lomonte, P., Baklouti, F. & Binda, O. The Biochemistry of Survival Motor Neuron Protein Is Paving the Way to Novel Therapies for Spinal Muscle Atrophy. *Biochemistry* **59**, 1391–1397 (2020).

34. Karyka, E. *et al.* SMN-deficient cells exhibit increased ribosomal DNA damage. *Life Sci. Alliance* **5**, e202101145 (2022).